

Unveiling AI’s Blind Spots: An Oracle for In-Domain, Out-of-Domain, and Adversarial Errors

Shuangpeng Han^{1 2} Mengmi Zhang^{1 2}

Abstract

AI models make mistakes when recognizing images—whether in-domain, out-of-domain, or adversarial. Predicting these errors is critical for improving system reliability, reducing costly mistakes, and enabling proactive corrections in real-world applications such as healthcare, finance, and autonomous systems. However, understanding what mistakes AI models make, why they occur, and how to predict them remains an open challenge. Here, we conduct comprehensive empirical evaluations using a “mentor” model—a deep neural network designed to predict another “mentee” model’s errors. Our findings show that the mentor excels at learning from a mentee’s mistakes on adversarial images with small perturbations and generalizes effectively to predict in-domain and out-of-domain errors of the mentee. Additionally, transformer-based mentor models excel at predicting errors across various mentee architectures. Subsequently, we draw insights from these observations and develop an “oracle” mentor model, dubbed SuperMentor, that can outperform baseline mentors in predicting errors across different error types from the ImageNet-1K dataset. Our framework paves the way for future research on anticipating and correcting AI model behaviors, ultimately increasing trust in AI systems. All code, models, and data will be made publicly available.

1. Introduction

AI models are prone to making errors in image recognition tasks, whether dealing with in-domain, out-of-domain

(OOD), or adversarial examples. In-domain errors occur when models misclassify familiar data within the training domain, while OOD errors arise when faced with unseen or out-of-domain data. Adversarial errors are particularly concerning, as they result from carefully crafted perturbations designed to mislead the model.

Accurately predicting these errors is critical to enhancing the robustness and reliability of AI, especially in high-stakes real-world applications such as healthcare (Habeheh & Gohel, 2021), finance (Mashrur et al., 2020), and autonomous driving (Huang et al., 2022). Proactively identifying potential errors enables more efficient corrections, reducing costly mistakes and safeguarding against catastrophic failures. By predicting when models are likely to err, we can implement strategies that either mitigate or entirely avoid the risks associated with those errors, ultimately leading to more trustworthy AI deployments.

Understanding the specific types of errors AI systems make, the reasons why they make these errors, and most importantly, how to predict these errors remains an unresolved challenge. Existing literature on error monitoring systems for AI models encompasses various approaches, including uncertainty estimation (Nado et al., 2021; Lakshminarayanan et al., 2017), anomaly detection (Bogdoll et al., 2022), outlier detection (Boukerche et al., 2020), and out-of-domain detection (Yang et al., 2024). While these methods are crucial for assessing model reliability, they mainly focus on determining whether a given data point falls outside the scope of the model’s training. Thus, these approaches misalign with our primary objective of predicting whether AI models will make mistakes, as models can err on familiar data while behaving correctly on out-of-scope samples.

Subsequent research in out-of-domain detection has demonstrated that a model’s accuracy is often correlated with how far the data deviates from in-domain samples (Hendrycks & Dietterich, 2019; Shankar et al., 2021; Li et al., 2017). These methods typically rely on predefined metrics, such as model parameter distances (Yu et al., 2022), model disagreements (Jiang et al., 2021; Madani et al., 2004) and confidence scores (Guillory et al., 2021), which limits their ability to generalize predictions

¹College of Computing and Data Science, Nanyang Technological University, Singapore ²Deep NeuroCognition Lab, Agency for Science, Technology and Research (A*STAR). Correspondence to: Mengmi Zhang <mengmi.zhang@ntu.edu.sg>.

Under review.

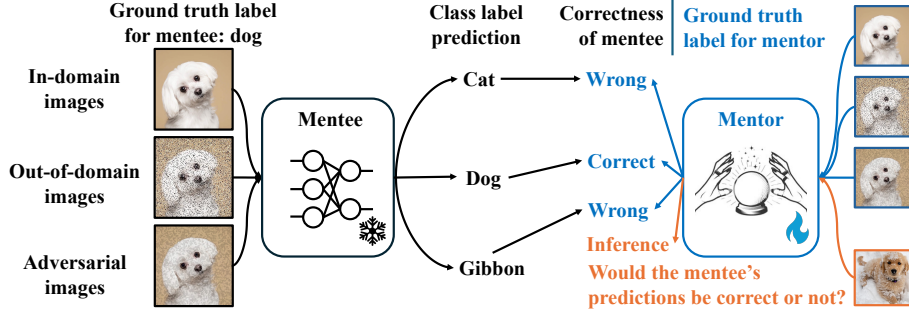


Figure 1. AI models make mistakes and an “oracle” mentor model predicts when they will happen. A “mentee” neural network (black) was trained for multi-class image recognition, but it can still misclassify in-domain, out-of-domain, and adversarial images. For instance, it might mislabel an in-domain dog image as a cat. The mentor model (blue), inputting the same images as the mentee, predicts whether the mentee will make a mistake. For example, if the mentee incorrectly labels an adversarial dog image, the mentor’s ground truth label is “wrong”; conversely, if the mentee correctly labels an out-of-domain dog image, the mentor’s label is “correct”. The mentee’s parameters are frozen (snowflake), while the mentor’s are trainable (fire). During inference (orange), the mentor predicts whether the mentee will make an error on test images that have never been seen by both the mentee and the mentor.

across various data types, including errors arising from in-domain data or adversarial attacks (Szegedy, 2013). In parallel, earlier efforts in trustworthiness prediction mostly depend on shallow neural networks (Corbière et al., 2019; Qiu & Miiikkulainen, 2022; Jiang et al., 2018) or carefully-designed loss functions (Luo et al., 2021). However, they do not investigate how different error types influence trustworthiness prediction.

Another line of research improves the robustness of the AI models with adversarial training approaches (Ilyas et al., 2019; Gowal et al., 2020; Balunović & Vechev, 2020); however, these approaches primarily focus on improving the model’s overall performance rather than predicting when errors may occur in the models. Moreover, unlike selective prediction (Geifman & El-Yaniv, 2017), rejection learning (Cortes et al., 2016), and learning to defer (Madras et al., 2018), which jointly train the selection/rejection function with the mentee, our method trains the mentor and mentee independently. This separation is especially beneficial when mentee training is time- and resource-intensive or when its training data is inaccessible.

Different from all these works, we delve into the underlying principles of errors generated by AI models in the task of image classification with another AI model. Specifically, we designate the AI model that predicts errors as the **mentor** and the AI model being evaluated for performance as the **mentee**. The mentor strives to predict whether the mentee makes a mistake for any given data. See Fig. 1 for the illustration of the problem setup. Training the mentor on the error patterns made by the mentee can potentially reveal the strengths and weaknesses of the mentee’s learned representations across various visual contexts.

Our main contributions are highlighted below:

1. We conduct an in-depth analysis of how training mentors on each of three distinct error types specified by the

mentees—In-Domain (ID) Errors, Out-of-Domain (OOD) Errors, and Adversarial Attack (AA) Errors—affect the performance of error predictions over three increasingly complex image datasets CIFAR-10 (Krizhevsky et al., 2009), CIFAR-100 (Krizhevsky et al., 2009) and ImageNet-1K (Deng et al., 2009). Our results reveal that training mentors with adversarial attack errors from the mentee has the most significant impact on improving the mentor’s error prediction accuracy.

2. We investigate how various mentor model architectures affect error prediction performance. Our experiments demonstrate that transformer-based mentor models outperform other architectures in predicting errors.

3. We explore how varying levels of distortion in OOD and adversarial images affect the accuracy of error predictions. The findings indicate that training mentors on images with small perturbations can improve error prediction accuracy. In addition, we show that a mentor trained to learn error patterns from one mentee can successfully generalize its error predictions to another mentee.

4. Based on our findings from points 1 to 3, we present the SuperMentor model, which predicts errors across diverse mentee architectures and error types. Experimental results show that SuperMentor outperforms baseline mentors, demonstrating its superior error-predictive capabilities.

2. Related work

Error monitoring systems for AI models. With the growing deployment of AI models across diverse fields, ensuring their reliability and understanding their limitations has become increasingly crucial. This has led to numerous research in safe AI such as uncertainty estimation (Nado et al., 2021; Lakshminarayanan et al., 2017), anomaly detection (Bogdoll et al., 2022), outlier detection (Boukerche et al., 2020) and out-of-domain

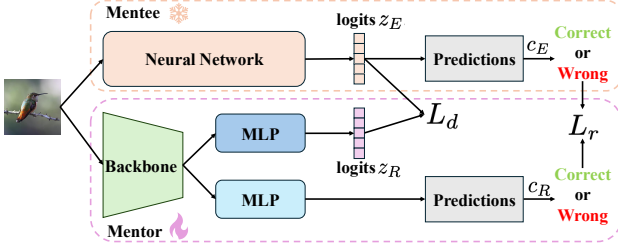


Figure 2. **Overview of a mentor model.** Given a fixed mentee model (snowflake), the mentor model takes an input image and uses a pre-trained backbone on ImageNet-1K (Deng et al., 2009) to extract features. The feature maps are then processed in two streams via multi-layer perceptrons (MLP)s. The output logits z_R from one stream are compared with the mentee’s output logits z_E using a distillation loss L_d . The other stream performs a binary prediction of whether the mentee makes a mistake or not. The prediction is supervised by a logistic regression loss L_r . The parameters of MLPs in the two streams are not shared.

detection (Yang et al., 2024). Unlike these areas, which mainly aim to predict whether the input data falls outside the training domain, our focus is on monitoring and predicting errors in AI models by determining whether the model’s output is correct, irrespective of whether the data comes from the training domain. To detect whether the input data is out of scope, the prior approaches mainly rely on softmax outputs (Granese et al., 2021; Hendrycks & Gimpel, 2016; Dang et al., 2024), activations from network layers (Wang et al., 2020; Cheng et al., 2019; Ferreira et al., 2023), shallow neural networks (Corbière et al., 2019; Qiu & Mikkilainen, 2022; Jiang et al., 2018), and carefully-designed loss functions (Luo et al., 2021) in applications such as object detection (Kang et al., 2018) and trajectory prediction (Shao et al., 2023; 2024). However, these methods often rely on manually defined metrics to estimate the likelihood of a mentee making mistakes, or they fail to examine how different error types affect error prediction. In contrast, our strategy employs a separate deep neural network to automatically learn and approximate the mentee’s decision boundaries for specific error types, providing an end-to-end trainable framework for error prediction. Moreover, our research direction differs from selective prediction (Geifman & El-Yaniv, 2017), rejection learning (Cortes et al., 2016), and learning to defer (Madras et al., 2018) by avoiding joint training with the mentee and requiring no knowledge of the mentee’s training data. Besides, although rejecting a mentee’s unreliable predictions and predicting the correctness of a mentee’s outputs are often positively correlated, they remain distinct tasks.

Out-of-domain detection. Our research on predicting mentee errors is closely related to out-of-domain detection in error monitoring systems, though it differs in several key aspects. As highlighted by (Guérin et al., 2023), error

prediction is distinct from OOD detection (Liu et al., 2020a; Sun et al., 2021; Lee et al., 2018; Sun et al., 2022) in their objectives. While OOD detection aims to detect whether the given data comes from the same domain as the training set, the aim of error prediction is to learn whether the mentee will make a mistake on the given data. In other words, out-of-domain data may not necessarily cause the model to err, and model errors can also occur on in-domain data.

Recent studies (Hendrycks & Dietterich, 2019; Shankar et al., 2021; Li et al., 2017) have shown that a model’s accuracy on a given dataset is often correlated with how far the data deviates from in-domain samples. However, these studies typically rely on pre-defined metrics, such as model parameter distances (Yu et al., 2022), model disagreements (Jiang et al., 2021; Madani et al., 2004), confidence scores (Guillory et al., 2021), domain-invariant representations (Chuang et al., 2020), and domain augmentation (Deng et al., 2021a), limiting their ability to generalize error prediction beyond in-domain data. In contrast, our mentor is capable of predicting both OOD and in-domain errors for a mentee. Additionally, our mentor is an AI model trained end-to-end without relying on manually defined criteria.

Adversarial attack and defense. In addition to OOD error, (Szegedy, 2013) discovered that deep neural networks can be fooled using input perturbations of extremely low magnitude. Building upon this finding, a substantial number of adversarial attacks have been proposed, including white-box attacks (Goodfellow et al., 2014; Mađry et al., 2017; Carlini & Wagner, 2017; Schwinn et al., 2023; Gao et al., 2020), black-box attacks (Uesato et al., 2018; Rahmati et al., 2020; Brendel et al., 2017; Chen et al., 2020), and backdoor attacks (Liu et al., 2020b; Xie et al., 2019; Kolouri et al., 2020). To defend against these adversarial attacks, various defence mechanisms (Qin et al., 2019; Deng et al., 2021b; Liu et al., 2019) have been developed to withstand or detect adversarial inputs. Furthermore, although the primary objective of adversarial attacks is to deceive AI models, there are instances where adversarial perturbations are exploited to enhance the model performance — a technique known as adversarial training (Ilyas et al., 2019; Goyal et al., 2020; Balunović & Vechev, 2020). Unlike adversarial training, which involves using adversarial samples to train the mentee, our approach focuses on teaching mentors to learn the mentee’s error patterns revealed by these adversarial attack samples.

3. Experimental setups

We denote the mentor and mentee networks as $f_R(\cdot)$ and $f_E(\cdot)$ respectively. We also define \mathcal{X} as the domain-specific set containing all the test images for a mentee, and \mathcal{Y} as their ground-truth object class labels. Therefore, a mentor is

expected to make perfect predictions about the correctness of the mentee’s responses (1 for “correct” and 0 for “wrong”) given any image x from \mathcal{X} :

$$\forall x \in \mathcal{X}, f_R(x) = \begin{cases} 1 & \text{if } f_E(x) = y, \\ 0 & \text{otherwise.} \end{cases} \quad (1)$$

where $y \in \mathcal{Y}$ is the ground-truth object class label of the corresponding image x .

3.1. Mentors

Model architecture: We propose mentor models, as illustrated in **Fig. 2**. Given an input image, the backbone of a mentor model extracts features from the input image. We adopt either of the two backbones for the feature extractors of mentors: a 2D Convolutional Neural Network (2D-CNN) ResNet50 (He et al., 2016) and a transformer-based ViT (Dosovitskiy, 2020). The extracted feature maps are further processed in two streams implemented as multi-layer perceptrons (MLP)s. The parameters of the MLPs in the two streams are not shared.

The first stream generates logits z_R by predicting the probability distribution of a mentee over all the object classes when the mentee classifies the given image. The mentee network is kept fixed while training the mentor. Let us define the mentee’s output logit as z_E . We introduce the distillation loss proposed by (Hinton, 2015): $L_d = T^2 \cdot KL(\sigma(\frac{z_E}{T}) || \sigma(\frac{z_R}{T}))$ to align z_R with z_E , where $KL(\cdot || \cdot)$ represents Kullback-Leibler divergence. $\sigma(\cdot)$ is the softmax function. $T = 1.0$ is the temperature, which controls the smoothness of the soft probability distribution.

In the second stream, the mentor is prompted to predict whether the mentee will make a mistake on the given image or not. We denote the predicted binary label as c_R , where 1 indicates that the mentee does not make a mistake and vice versa for 0. This prediction is supervised by $L_r = -[c_E \log(z_p) + (1 - c_E) \log(1 - z_p)]$, where c_E is the ground truth correctness label of a mentee and z_p represents the mentor’s predicted probability that the mentee’s prediction is correct. The overall loss is $L = L_d + L_r$.

Training and implementation details: All mentors are trained on Nvidia RTX A5000 and A6000 GPUs, utilizing the AdamW optimizer (Loshchilov & Hutter, 2017) with a cosine annealing scheduler (Loshchilov & Hutter, 2016), and an initial learning rate of 2×10^{-4} . All mentors load the weights of the feature extractor pre-trained on the ImageNet-1K dataset for 1000-way image classification tasks (Deng et al., 2009) and further fine-tune on the error prediction task. During training, images are resized and center-cropped to 224×224 pixels. All the mentor models are trained for 40 epochs with a batch size of 512.

3.2. Mentees and their datasets

We employ two architectures as the mentees’ backbones: ResNet50 (He et al., 2016), which is a 2D-Convolutional neural network (2D-CNN), and ViT (Dosovitskiy, 2020), which is a transformer based on self-attention mechanisms.

To train and test our mentees, we include three image datasets of varying sizes and follow their standard data splits: CIFAR-10 (C10, (Krizhevsky et al., 2009)) with 10 object classes, CIFAR-100 with 100 object classes (C100, (Krizhevsky et al., 2009)) and ImageNet-1K with 1000 object classes (IN, (Deng et al., 2009)). The multi-class recognition accuracy on the standard test sets of C10, C100 and IN datasets are 96.98%, 84.54%, 76.13% for the ResNet50 mentee and 97.45%, 86.51%, 81.07% for the ViT mentee respectively. The parameters of the mentees are frozen in all the experiments conducted on mentors.

3.3. Datasets for training and testing mentors

The mentor’s objective is to predict whether the mentee will misclassify a given image, regardless of its source. The mentor is trained on correctly and wrongly classified images by a mentee. Next, we introduce how these images are curated and collected. A mentee may encounter various types of errors when dealing with real-world data. To explore which error types most effectively reveal the mentee’s learning patterns, we categorize errors into three types: (1) errors from in-domain images, (2) errors from out-of-domain images, and (3) errors from adversarial images generated by adversarial attacks. Next, we introduce these three error types in detail.

In-Domain (ID) Errors occur on data that come from the same domain as the mentee’s training dataset. Specifically, errors on images from the standard validation set of ImageNet-1K or the test sets of CIFAR-10 and CIFAR-100 are considered ID errors. Along with the correctly classified images from these standard test sets, we create three datasets for a mentor: **IN-ID**, **C10-ID**, and **C100-ID**, following the naming convention of [Dataset]-[Error Type].

Out-of-domain (OOD) Errors refer to errors that arise when the mentee encounters data outside the training domain. To obtain OOD samples of a dataset, we adopt four types of image corruptions from (Hendrycks & Dietterich, 2019): **speckle noise (SpN)** (noise category), **Gaussian blur (GaB)** (blur category), **spatter (Spat)** (weather category), and **saturate (Sat)** (digital category). The noise levels can vary and we select level 1 for image corruptions as specified in (Hendrycks & Dietterich, 2019) by default. As noise levels increase, distortions on OOD images become more pronounced, causing the mentee to make more errors.

Following the naming conventions of [Dataset]-[Error Type]-[Error Source], we collect correctly and wrongly

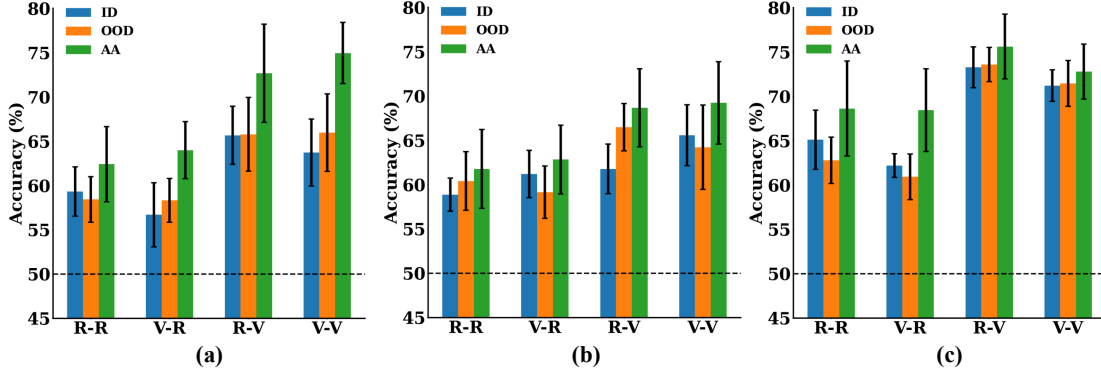


Figure 3. Mentors trained on adversarial images of a mentee outperform mentors trained on OOD and ID images of the same mentee. Average accuracy of a mentor trained on one type of error of a mentee for (a) CIFAR-10, (b) CIFAR-100 and (c) ImageNet-1K datasets is presented. Three types of errors made by a mentee are categorized based on in-domain (ID, blue), out-of-domain (OOD, orange), and images generated by adversarial attacks (AA, green). In each subplot, the labels on the x-axis are interpreted as [mentee]-[mentor], where ‘V’ and ‘R’ represent ViT and ResNet50 architectures for a mentee or a mentor respectively. Error bars indicate the standard deviation. The dotted black line indicates the chance level. See Sec. 3.3 and Sec. 3.4 for error types and the evaluation metric. The four sets of bars in each subfigure correspond to the heatmaps shown in subfigures (a), (b), (c), and (d) of Appendix, Fig. S3- S5.

classified OOD samples based on C10 images of a mentee and curate four datasets for a mentor: **C10-OOD-SpN**, **C10-OOD-GaB**, **C10-OOD-Spat** and **C10-OOD-Sat**. Without the loss of generality, we can also curate four datasets each for a mentor based on C100 and IN images of a mentee.

Adversarial Attack (AA) Errors. Errors from adversarial images are specifically generated by adversarial attack methods to mislead or confuse the mentee. Given our assumption that the mentor has full access to the student model’s parameters, we focus exclusively on white-box adversarial attacks as they typically produce more subtle yet effective perturbations compared to their black-box counterparts. To generate adversarial images, we employ four untargeted adversarial attack methods: **PGD** (Mądry et al., 2017) creates adversarial examples by repeatedly taking steps along the loss gradient; **CW** (Carlini & Wagner, 2017) attempts to minimize the L_2 norm of the perturbation while ensuring misclassification. **Jitter** (Schwinn et al., 2023) adds Gaussian noise to the output logits to encourage a diverse set of target classes for the attack. **PIFGSM** (Gao et al., 2020) crafts patch-wise noise instead of pixel-wise noise. We set $c = 1.0$ in the CW attack, and perturbation bound $\epsilon = \frac{1}{255}$ for other attacks by default. See their papers for these hyper-parameter definitions. Intuitively, the attacks are stronger with higher hyper-parameter values; hence, the mentees make more mistakes.

Note that adversarial attacks are not always successful, and mentees can still correctly classify some adversarial images. We collect both the correctly and incorrectly classified adversarial images by a mentee based on C10 images, curating four datasets for the mentor: **C10-AA-PGD**, **C10-AA-CW**, **C10-AA-Jitter**, **C10-AA-PIFGSM**. Similarly, we can also curate four datasets each for a mentor

based on C100 and IN images of a mentee.

Training and test splits. The number of correctly and incorrectly classified images by a mentee can vary significantly based on its classification performance. To create balanced training and test sets for the mentor and avoid the long-tailed distribution problem, we select an equal number of correctly and incorrectly classified samples for each training batch and every test set. See Appendix, Sec. A for more details.

3.4. Baselines and evaluation metric

Baselines. We include seven baseline methods for error prediction of a mentee. 1) **Self Error Rate (SER)** predicts the correctness of the mentee’s outputs by randomly assigning “correct” or “wrong” based on the mentee’s in-domain accuracy; 2) **Maximum Class Probability (MCP)** (Hendrycks & Gimpel, 2016) classify the mentee’s predictions as correct if its MCP exceeds a predefined threshold. 3) **Class Probability Entropy (CPE)** evaluates a mentee’s prediction as correct if its entropy of the probability distribution over all classes is below a predefined threshold. 4) **Distance To Centroid (DTC)** considers a prediction correct if its feature embedding is within a predefined distance from the class centroid. 5) **ConfidNet** (Corbière et al., 2019) predicts failure by learning True Class Probability (TCP) on the training samples. 6) **TrustScore** (Jiang et al., 2018) employs Trust Score to quantify the agreement between the classifier and a modified nearest-neighbor classifier. 7) **Steep Slope Loss (SSL)** (Luo et al., 2021) develops a neural network for predicting trustworthiness by utilizing a steep slope loss function. See Appendix, Sec. B for more details.

Evaluation metric. To assess the performance of mentors,

we report their error prediction accuracy on the test set corresponding to each specified error source. For instance, a mentor trained on the C10-ID training set is evaluated on the C10-OOD-SpN test set. The error prediction accuracy is calculated by averaging the mentor’s accuracies on the samples that the mentee correctly classified and those that the mentee incorrectly classified. However, since a mentee can make mistakes across various real-world scenarios, a mentor must accurately predict errors across all error types. Therefore, we compute the average accuracy, named as *Accuracy (%)* of a mentor across all test sets, including one ID error, four OOD errors, and four AA errors. See **Appendix, Sec. C** for an example calculation of the average accuracy of a mentor.

4. Results

4.1. Training on specific errors of mentees impacts the performance of mentors

A mentee’s mistakes can reveal their learning biases, behaviors, or traits. Here, we investigate which types of errors offer the most insight into understanding a mentee’s decision boundaries during image recognition tasks. We train mentors with identical architectures on datasets containing specific error types made by the mentee across C10 (**Fig. 3(a)**), C100 (**Fig. 3(b)**), and IN (**Fig. 3(c)**). For instance, if a mentor trained on C10-OOD achieves higher accuracy in error prediction compared to one trained on C10-IN, this suggests that in-domain errors provide less diagnostic information about the mentee’s decision-making process than out-of-domain errors. Both mentors and mentees may have the same or different backbones, such as ResNet50 (R) or ViT (V).

As shown in **Fig. 3**, over C10, C100, and IN images, the high accuracy for mentors trained on adversarial attack (AA) errors indicates that these errors offer deeper insights into the mentee’s decision process compared to out-of-domain (OOD) and in-domain (ID) errors. In some cases, mentors trained on OOD errors slightly outperformed those trained on ID errors, though both were still inferior to those trained on AA errors. Interestingly, our experiments reveal that training mentors exclusively on AA errors performs marginally worse than joint training on ID, OOD, and AA errors (see **Appendix, Sec. D**). This result underscores a significant overlap of mentee error patterns among ID, OOD, and AA data.

Loss landscape analysis. A loss landscape of a mentee reflects how a mentee’s loss function behaves across different parameter configurations. Mentors’ performance offers insights into the structure of a mentee’s loss landscape. Consistent with (Ilyas et al., 2019), the high accuracy of mentors trained on AA errors suggests that adversarial

images lie closer to the mentee’s decision boundary, enabling more accurate prediction of the mentee’s mistakes and a deeper understanding of the loss landscape. Similarly, OOD data aids mentors in learning boundaries by shifting ID samples closer to the boundary. However, it does not explore the boundary as thoroughly as adversarial images. ID data, with fewer samples near the boundary, provides more limited exploration compared to adversarial images.

4.2. Mentor architectures matter in error predictions

To computationally model the decision boundary of a mentee using a mentor, the mentor requires more complex architectures with a larger number of parameters than the mentee. Indeed, from **Fig. 3**, over all the datasets, we observed that utilizing ViT (V) as the mentor backbone consistently achieves higher accuracy across all error types of ViT-based and ResNet-based mentees compared to the mentor based on ResNet50 (R). One example of this performance disparity is observed in the context of the adversarial attack error type for CIFAR-10. The ViT-based mentor attains an accuracy of 74.95%, substantially higher than the accuracy of 63.99% for the ResNet-based mentor.

Loss landscape analysis. The performance difference between mentors’ architectures is due to ViT’s superior ability to identify features from error patterns. Its self-attention mechanism captures complex relationships among data samples, providing a deeper understanding of the mentee’s loss landscape, particularly in modelling irregular, rugged landscapes with sharp peaks and valleys.

4.3. Training on images with smaller perturbations helps error predictions

Although adversarial images have been demonstrated to aid in error prediction (**Sec. 4.1**), it remains unclear whether adversarial images with varying degrees of image distortion exhibit the same effect. A straightforward method to regulate the level of image distortion caused by adversarial attacks is to set the perturbation bound ϵ . We employ four corruption levels by setting $\epsilon = \frac{1}{255}, \frac{2}{255}, \frac{4}{255},$ and $\frac{8}{255}$. We use the adversarial attack PIFGSM as an example since the error patterns from PIFGSM are most effective for the mentor’s prediction (see **Appendix, Fig. S3-S5**). As shown in **Fig. 4**, the mentor’s accuracy significantly decreases as the distortion level increases. In particular, for the C10-AA-PIFGSM, the accuracy at level 1 is 78.0%, which is notably higher than 51.7% at level 4. Our findings suggest that adversarial attacks employing smaller perturbations yield more benefits for mentor error prediction. This phenomenon can be attributed to the fact that adversarial images with minimal perturbations maintain closer proximity to the decision boundary of a mentee.

Building on the findings above, we investigate whether the

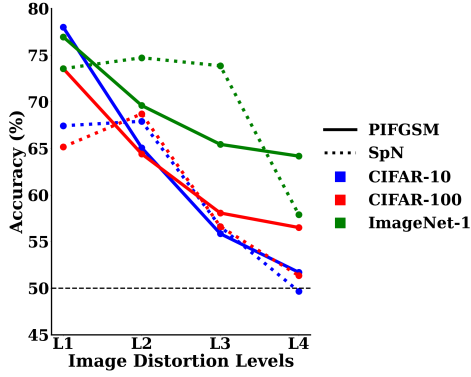


Figure 4. A mentor’s accuracy is heavily influenced by the levels of image distortions introduced by out-of-domain perturbations and adversarial attacks. ViT mentor’s accuracy is a function of varying image distortion levels from PIFGSM (Gao et al., 2020) and Speckle Noise (SpN) (Hendrycks & Dietterich, 2019) to the C10 images of a ResNet50-based mentee. The black dashed line indicates the chance level.

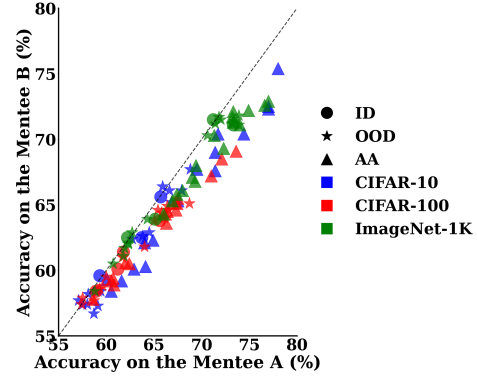


Figure 5. Mentors can generalize their error predictions across different mentee architectures. Mentors trained on mentee A’s predictions (x-axis) are evaluated against the predictions from mentee B (y-axis). Each marker is a generalization experiment of a mentor trained on different error types (marker shapes) in different image datasets (colours) of a mentee. The black dash line indicates the diagonal.

Table 1. Performance comparison of baselines and our SuperMentor on various types of errors from the ImageNet-1K dataset. The ResNet50 model serves as the mentee, with its correctness of predictions evaluated by mentors. Best results are in bold. Baseline performances across multiple hyperparameter configurations are detailed in Appendix, Tab. S2, while only the best configurations are presented here. The performance comparison with ViT mentee is shown in Appendix, Tab. S3.

	ID	SpN	GaB	Spat	Sat	PGD	CW	Jitter	PIFGSM	Average
SER	50.2	49.8	49.9	50.1	49.9	50.1	49.9	49.9	49.9	50.0
MCP ($\gamma = 0.7$)	77.3	76.8	77.4	78.3	76.6	71.8	72.9	71.7	69.4	74.7
CPE ($\alpha = 0.1$)	78.0	75.2	75.9	78.0	76.2	72.2	72.8	72.7	69.3	74.5
DTC ($d = 10$)	52.4	51.2	52.9	52.7	52.5	51.4	51.6	51.7	51.6	52.0
ConfidNet (Corbière et al., 2019)	67.3	65.9	68.5	70.8	67.9	68.8	69.0	70.1	67.1	68.4
TrustScore (Jiang et al., 2018)	70.0	67.5	71.1	73.4	71.3	73.2	72.5	73.9	72.7	71.7
SSL (Luo et al., 2021)	66.3	66.7	69.7	71.9	70.0	69.1	70.1	70.2	66.7	69.0
SuperMentor (ours)	78.9	73.6	74.6	78.3	73.6	83.0	78.4	79.9	72.3	77.0

mentor’s performance is influenced by how far OOD images are from the ID data. Specifically, we aim to determine whether the degree of deviation from the training domain impacts the mentor in a similar way to our observations on adversarial images. To explore this, we analyze images corrupted with Speckle Noise (SpN) and adjust the standard deviation σ of SpN to 0.01, 0.06, 0.15, and 0.6, representing four distinct levels of distortion. The outcomes are depicted in Fig. 4. We observe that the mentor’s accuracy improves as the distortion introduced by SpN decreases. For example, the mentor achieves an accuracy of 67.42% on level 1 of C10-OOD-SpN, while the accuracy drops significantly to 49.66% on level 4 of C100-OOD-SpN. This suggests that OOD error types with smaller perturbations enhance the mentor’s performance. However, unlike adversarial attacks, caution is necessary because the mentor’s accuracy can plateau with extremely small distortion levels, as shown by the minimal difference in accuracy between levels 1 and 2 of SpN in Fig. 4.

4.4. Mentors generalize across mentees

In Sec. 4.1, mentors have demonstrated their ability to learn the error patterns of mentees. This observation raises an important question: can the error patterns learned from one mentee (mentee A) be generalized to another mentee (mentee B) when the two mentees employ different model architectures? To explore this, we evaluate all 324 mentors, whose performances are depicted in Appendix, Tab. S6- S8, on the alternate mentee. Specifically, mentors trained on the errors of the ResNet50 mentee are tested on the predictions of the ViT mentee, and vice versa. The outcomes of these evaluations are illustrated in Fig. 5. Surprisingly, most points lie near the dashed diagonal line, implying that the mentors’ performance does not significantly deteriorate when evaluated on the predictions of different mentee architectures. This finding indicates that ResNet50 and ViT mentees tend to produce similar error patterns when trained on the same dataset.

4.5. Our SuperMentor outperforms all baselines

By drawing insights from observations in the subsections above, we propose an “oracle” mentor model, dubbed SuperMentor. We introduce the technical novelties of our SuperMentor below. First, as demonstrated in **Sec. 4.1** and **Sec. 4.3**, mentors trained on adversarial images with small perturbations of a mentee outperform those trained on OOD and ID images; thus, our SuperMentor adopts the training data from the PIFGSM error source of mentees with $\epsilon = \frac{1}{255}$. Second, since ViT has been proven to be a more effective architecture for mentors than ResNet50 (**Sec. 4.2**), SuperMentor adopts ViT as the backbone architecture.

We demonstrate the effectiveness of SuperMentor by comparing it with baselines introduced in **Sec. 3.4**. The results are shown in **Tab. 1**. It can be seen that our SuperMentor consistently achieves higher average accuracies over all error types compared to all baselines. Notably, in the AA scenarios, SuperMentor has significantly higher accuracy than the baselines. For example, SuperMentor achieves an error prediction accuracy of 83.0% on IN-AA-PGD of the ResNet50 mentee, whereas the best baseline only reaches 73.3%.

Baseline methods like SER, MCP, CPE, and DTC rely on fixed thresholds or predetermined values of manually defined criteria such as confidence or entropy, making them less adaptable to OOD and AA scenarios. In contrast, SuperMentor leverages deep neural networks to capture the complexity of error prediction. Additionally, methods like ConfidNet, TrustScore, and SSL are trained on ID error types. As shown in **Tab. 1**, these baselines are inferior to SuperMentor, which is trained exclusively on AA data. This suggests that the source of error data used to train the mentor plays a more critical role than the choice of loss functions or the sophisticated training strategies in these baselines.

We conduct extra network analysis of our SuperMentor. Specifically, we include an ablation study on the distillation loss L_d (**Appendix, Sec. F**). The removal of L_d leads to a significant drop in Accuracy, highlighting the importance of L_d . Moreover, we provide the visualization of SuperMentor’s embeddings based on the correctness of a mentee’s prediction across three error types (**Appendix, Sec. G**). Two distinct clusters are observed between samples wrongly or correctly classified by the mentee. This suggests that our SuperMentor is capable of accurately predicting the errors of a mentee regardless of the error sources.

5. Discussion and Conclusion

In our work, we tackle the challenge of predicting errors of AI models through extensive empirical evaluations using an end-to-end trainable “mentor” model. This mentor is designed to assess the correctness of a

mentee’s predictions across three distinct error types: in-domain errors, out-of-domain errors, and adversarial attack errors. Our results show that the mentor excels at learning from a mentee’s errors on adversarial images with minimal perturbations and, surprisingly, generalizes well to both in-domain and out-of-domain predictions of the same mentee. Additionally, we highlight the effectiveness of transformer-based mentor architectures compared to 2D-CNN-based ones, demonstrating their superior generalization capabilities across mentees with diverse backbones. Lastly, we introduce the SuperMentor, which outperforms all existing mentor baselines.

Despite the promising results, our framework may raise concerns regarding the vulnerabilities of AI mentors. Indeed, vulnerability is a well-known challenge for all Deep Neural Network (DNN)-based systems, yet this has not hindered their transformative applications in the real world. For example, DNNs are used to detect diabetic retinopathy (Jumper et al., 2021; Alyoubi et al., 2020), outperforming traditional diagnostic methods. Similarly, our work uses one AI to diagnose the other AI, which is a valid and impactful use case. To demonstrate its real-world utility, we extended our experiments to a medical image classification task for colorectal cancer diagnosis (**Appendix, Sec. H**). Our mentor achieves high error prediction accuracy compared to all competitive baselines, showcasing its practical uses in high-stake applications. More importantly, beyond the OOD domains evaluated in **Sec. 4.5**, results in **Appendix, Sec. I** show that our SuperMentor remains robust to mentee error patterns across an additional set of five unseen OOD domains. Moreover, the vulnerabilities of the mentor AI do not overlap with those of the mentees since mentors operate independently of the mentee’s architecture or training details, reducing the risk of shared weaknesses. To validate this point, we use EigenCAM to visualize the behavior of both our ViT SuperMentor and ViT mentee on example images (**Appendix, Fig. S2**). From **Fig. S2 (a)**, the mentor does not merely replicate the mentee’s learning patterns, as their activation maps for identical input images can differ significantly. Interestingly, our AI mentor can even serve as a valuable diagnostic tool for the AI mentees. In **Appendix, Fig. S2 (b)**, the mentor highlights the key feature pattern diagnostic for object recognition that the mentee tends to overlook. This suggests that the mentor can identify vulnerabilities in DNN-based models.

Our work paves the way for several promising research directions in safe and trustworthy AI. First, while our current research focuses on image classification, there is potential to extend this approach to other vision and language tasks, such as object detection and machine translation. Second, future research could explore mutual learning between mentors and mentees, where mentors not only learn from the mentee’s

error patterns but also provide valuable feedback to help refine the mentee. Third, we can establish more rigorous evaluation criteria for mentors, broadening their predictive capabilities. For example, beyond predicting whether a mentee is likely to make errors, mentors could also forecast the specific types of errors a mentee may encounter. Fourth, drawing parallels with AI mentors for AI mentees, we can explore the possibility of using AI mentors to investigate recognition errors in humans and primates. Such studies could provide insights into error pattern alignment between biological and artificial intelligent systems.

Impact Statement

As AI integrates into our daily lives and critical applications like healthcare, finance, and autonomous driving, ensuring its safety and reliability is imperative. Our research highlights the error patterns and characteristics of AI models for object recognition, paving the way for building trustworthy AI. By enabling one AI model to anticipate and correct another’s behavior, our framework helps ensure AI systems operate in a more predictable and reliable manner. Overall, our work lays the foundation for developing systems capable of anticipating the errors of others, offering practical value in high-stakes real-world applications.

References

- Alyoubi, W. L., Shalash, W. M., and Abulkhair, M. F. Diabetic retinopathy detection through deep learning techniques: A review. *Informatics in Medicine Unlocked*, 20:100377, 2020.
- Balunović, M. and Vechev, M. Adversarial training and provable defenses: Bridging the gap. In *8th International Conference on Learning Representations (ICLR 2020)(virtual)*. International Conference on Learning Representations, 2020.
- Bogdoll, D., Nitsche, M., and Zöllner, J. M. Anomaly detection in autonomous driving: A survey. In *Proceedings of the IEEE/CVF conference on computer vision and pattern recognition*, pp. 4488–4499, 2022.
- Boukerche, A., Zheng, L., and Alfandi, O. Outlier detection: Methods, models, and classification. *ACM Computing Surveys (CSUR)*, 53(3):1–37, 2020.
- Brendel, W., Rauber, J., and Bethge, M. Decision-based adversarial attacks: Reliable attacks against black-box machine learning models. *arXiv preprint arXiv:1712.04248*, 2017.
- Carlini, N. and Wagner, D. Towards evaluating the robustness of neural networks. In *2017 IEEE Symposium on Security and Privacy (SP)*, pp. 39–57. Ieee, 2017.
- Chen, W., Zhang, Z., Hu, X., and Wu, B. Boosting decision-based black-box adversarial attacks with random sign flip. In *European Conference on Computer Vision*, pp. 276–293. Springer, 2020.
- Cheng, C.-H., Nührenberg, G., and Yasuoka, H. Runtime monitoring neuron activation patterns. In *2019 Design, Automation & Test in Europe Conference & Exhibition (DATE)*, pp. 300–303. IEEE, 2019.
- Chuang, C.-Y., Torralba, A., and Jegelka, S. Estimating generalization under distribution shifts via domain-invariant representations. *arXiv preprint arXiv:2007.03511*, 2020.
- Corbière, C., Thome, N., Bar-Hen, A., Cord, M., and Pérez, P. Addressing failure prediction by learning model confidence. *Advances in Neural Information Processing Systems*, 32, 2019.
- Cortes, C., DeSalvo, G., and Mohri, M. Learning with rejection. In *Algorithmic Learning Theory: 27th International Conference, ALT 2016, Bari, Italy, October 19-21, 2016, Proceedings 27*, pp. 67–82. Springer, 2016.
- Dang, K. T., Delmas, K., Guiochet, J., and Guérin, J. Can we defend against the unknown? an empirical study about threshold selection for neural network monitoring. *arXiv preprint arXiv:2405.08654*, 2024.
- Deng, J., Dong, W., Socher, R., Li, L.-J., Li, K., and Fei-Fei, L. Imagenet: A large-scale hierarchical image database. In *2009 IEEE conference on computer vision and pattern recognition*, pp. 248–255. Ieee, 2009.
- Deng, W., Gould, S., and Zheng, L. What does rotation prediction tell us about classifier accuracy under varying testing environments? In *International Conference on Machine Learning*, pp. 2579–2589. PMLR, 2021a.
- Deng, Z., Yang, X., Xu, S., Su, H., and Zhu, J. Libre: A practical bayesian approach to adversarial detection. In *Proceedings of the IEEE/CVF conference on computer vision and pattern recognition*, pp. 972–982, 2021b.
- Dosovitskiy, A. An image is worth 16x16 words: Transformers for image recognition at scale. *arXiv preprint arXiv:2010.11929*, 2020.
- Ferreira, R. S., Guerin, J., Guiochet, J., and Waeselyneck, H. Sena: Similarity-based error-checking of neural activations. In *ECAI 2023*, pp. 724–731. IOS Press, 2023.
- Gao, L., Zhang, Q., Song, J., Liu, X., and Shen, H. T. Patch-wise attack for fooling deep neural network. In *Computer Vision—ECCV 2020: 16th European Conference, Glasgow, UK, August 23–28, 2020, Proceedings, Part XXVIII 16*, pp. 307–322. Springer, 2020.

- Geifman, Y. and El-Yaniv, R. Selective classification for deep neural networks. *Advances in neural information processing systems*, 30, 2017.
- Gildenblat, J. and contributors. Pytorch library for cam methods. <https://github.com/jacobgil/pytorch-grad-cam>, 2021.
- Goodfellow, I. J., Shlens, J., and Szegedy, C. Explaining and harnessing adversarial examples. *arXiv preprint arXiv:1412.6572*, 2014.
- Gowal, S., Qin, C., Huang, P.-S., Cemgil, T., Dvijotham, K., Mann, T., and Kohli, P. Achieving robustness in the wild via adversarial mixing with disentangled representations. In *Proceedings of the IEEE/CVF Conference on Computer Vision and Pattern Recognition*, pp. 1211–1220, 2020.
- Granese, F., Romanelli, M., Gorla, D., Palamidessi, C., and Piantanida, P. Doctor: A simple method for detecting misclassification errors. *Advances in Neural Information Processing Systems*, 34:5669–5681, 2021.
- Guérin, J., Delmas, K., Ferreira, R., and Guiochet, J. Out-of-distribution detection is not all you need. In *Proceedings of the AAAI conference on artificial intelligence*, volume 37, pp. 14829–14837, 2023.
- Guillory, D., Shankar, V., Ebrahimi, S., Darrell, T., and Schmidt, L. Predicting with confidence on unseen distributions. In *Proceedings of the IEEE/CVF international conference on computer vision*, pp. 1134–1144, 2021.
- Habebh, H. and Gohel, S. Machine learning in healthcare. *Current genomics*, 22(4):291, 2021.
- He, K., Zhang, X., Ren, S., and Sun, J. Deep residual learning for image recognition. In *Proceedings of the IEEE conference on computer vision and pattern recognition*, pp. 770–778, 2016.
- Hendrycks, D. and Dietterich, T. Benchmarking neural network robustness to common corruptions and perturbations. *arXiv preprint arXiv:1903.12261*, 2019.
- Hendrycks, D. and Gimpel, K. A baseline for detecting misclassified and out-of-distribution examples in neural networks. *arXiv preprint arXiv:1610.02136*, 2016.
- Hendrycks, D., Basart, S., Mu, N., Kadavath, S., Wang, F., Dorundo, E., Desai, R., Zhu, T., Parajuli, S., Guo, M., et al. The many faces of robustness: A critical analysis of out-of-distribution generalization. In *Proceedings of the IEEE/CVF international conference on computer vision*, pp. 8340–8349, 2021.
- Hinton, G. Distilling the knowledge in a neural network. *arXiv preprint arXiv:1503.02531*, 2015.
- Huang, Y., Du, J., Yang, Z., Zhou, Z., Zhang, L., and Chen, H. A survey on trajectory-prediction methods for autonomous driving. *IEEE Transactions on Intelligent Vehicles*, 7(3):652–674, 2022.
- Ilyas, A., Santurkar, S., Tsipras, D., Engstrom, L., Tran, B., and Madry, A. Adversarial examples are not bugs, they are features. *Advances in neural information processing systems*, 32, 2019.
- Jiang, H., Kim, B., Guan, M., and Gupta, M. To trust or not to trust a classifier. *Advances in neural information processing systems*, 31, 2018.
- Jiang, Y., Nagarajan, V., Baek, C., and Kolter, J. Z. Assessing generalization of sgd via disagreement. *arXiv preprint arXiv:2106.13799*, 2021.
- Jumper, J., Evans, R., Pritzel, A., Green, T., Figurnov, M., Ronneberger, O., Tunyasuvunakool, K., Bates, R., Žídek, A., Potapenko, A., et al. Highly accurate protein structure prediction with alphafold. *nature*, 596(7873):583–589, 2021.
- Kang, D., Raghavan, D., Bailis, P., and Zaharia, M. Model assertions for debugging machine learning. In *NeurIPS MLSys Workshop*, volume 3, 2018.
- Kather, J. N., Krisam, J., Charoentong, P., Luedde, T., Herpel, E., Weis, C.-A., Gaiser, T., Marx, A., Valous, N. A., Ferber, D., et al. Predicting survival from colorectal cancer histology slides using deep learning: A retrospective multicenter study. *PLoS medicine*, 16(1): e1002730, 2019.
- Kolouri, S., Saha, A., Pirsiavash, H., and Hoffmann, H. Universal litmus patterns: Revealing backdoor attacks in cnns. In *Proceedings of the IEEE/CVF Conference on Computer Vision and Pattern Recognition*, pp. 301–310, 2020.
- Krizhevsky, A., Hinton, G., et al. Learning multiple layers of features from tiny images. 2009.
- Lakshminarayanan, B., Pritzel, A., and Blundell, C. Simple and scalable predictive uncertainty estimation using deep ensembles. *Advances in neural information processing systems*, 30, 2017.
- Lee, K., Lee, K., Lee, H., and Shin, J. A simple unified framework for detecting out-of-distribution samples and adversarial attacks. *Advances in neural information processing systems*, 31, 2018.

- Li, D., Yang, Y., Song, Y.-Z., and Hospedales, T. M. Deeper, broader and artier domain generalization. In *Proceedings of the IEEE international conference on computer vision*, pp. 5542–5550, 2017.
- Liu, J., Zhang, W., Zhang, Y., Hou, D., Liu, Y., Zha, H., and Yu, N. Detection based defense against adversarial examples from the steganalysis point of view. In *Proceedings of the IEEE/CVF Conference on Computer Vision and Pattern Recognition*, pp. 4825–4834, 2019.
- Liu, W., Wang, X., Owens, J., and Li, Y. Energy-based out-of-distribution detection. *Advances in neural information processing systems*, 33:21464–21475, 2020a.
- Liu, Y., Ma, X., Bailey, J., and Lu, F. Reflection backdoor: A natural backdoor attack on deep neural networks. In *Computer Vision–ECCV 2020: 16th European Conference, Glasgow, UK, August 23–28, 2020, Proceedings, Part X 16*, pp. 182–199. Springer, 2020b.
- Loshchilov, I. and Hutter, F. Sgdr: Stochastic gradient descent with warm restarts. *arXiv preprint arXiv:1608.03983*, 2016.
- Loshchilov, I. and Hutter, F. Decoupled weight decay regularization. *arXiv preprint arXiv:1711.05101*, 2017.
- Luo, Y., Wong, Y., Kankanhalli, M. S., and Zhao, Q. Learning to predict trustworthiness with steep slope loss. *Advances in Neural Information Processing Systems*, 34: 21533–21544, 2021.
- Madani, O., Pennock, D., and Flake, G. Co-validation: Using model disagreement on unlabeled data to validate classification algorithms. *Advances in neural information processing systems*, 17, 2004.
- Madras, D., Pitassi, T., and Zemel, R. Predict responsibly: improving fairness and accuracy by learning to defer. *Advances in neural information processing systems*, 31, 2018.
- Mađry, A., Makelov, A., Schmidt, L., Tsipras, D., and Vladu, A. Towards deep learning models resistant to adversarial attacks. *stat*, 1050(9), 2017.
- Mashrur, A., Luo, W., Zaidi, N. A., and Robles-Kelly, A. Machine learning for financial risk management: a survey. *Ieee Access*, 8:203203–203223, 2020.
- Muhammad, M. B. and Yeasin, M. Eigen-cam: Class activation map using principal components. In *2020 international joint conference on neural networks (IJCNN)*, pp. 1–7. IEEE, 2020.
- Nado, Z., Band, N., Collier, M., Djolonga, J., Dusenberry, M. W., Farquhar, S., Feng, Q., Filos, A., Havasi, M., Jenatton, R., et al. Uncertainty baselines: Benchmarks for uncertainty & robustness in deep learning. *arXiv preprint arXiv:2106.04015*, 2021.
- Qin, Y., Frosst, N., Sabour, S., Raffel, C., Cottrell, G., and Hinton, G. Detecting and diagnosing adversarial images with class-conditional capsule reconstructions. *arXiv preprint arXiv:1907.02957*, 2019.
- Qiu, X. and Miikkulainen, R. Detecting misclassification errors in neural networks with a gaussian process model. In *Proceedings of the AAAI Conference on Artificial Intelligence*, volume 36, pp. 8017–8027, 2022.
- Rahmati, A., Moosavi-Dezfooli, S.-M., Frossard, P., and Dai, H. Geoda: a geometric framework for black-box adversarial attacks. In *Proceedings of the IEEE/CVF conference on computer vision and pattern recognition*, pp. 8446–8455, 2020.
- Schwinn, L., Raab, R., Nguyen, A., Zanca, D., and Eskofier, B. Exploring misclassifications of robust neural networks to enhance adversarial attacks. *Applied Intelligence*, 53 (17):19843–19859, 2023.
- Shankar, V., Dave, A., Roelofs, R., Ramanan, D., Recht, B., and Schmidt, L. Do image classifiers generalize across time? In *Proceedings of the IEEE/CVF International Conference on Computer Vision*, pp. 9661–9669, 2021.
- Shao, W., Li, J., and Wang, H. Self-aware trajectory prediction for safe autonomous driving. In *2023 IEEE Intelligent Vehicles Symposium (IV)*, pp. 1–8. IEEE, 2023.
- Shao, W., Li, B., Yu, W., Xu, J., and Wang, H. When is it likely to fail? performance monitor for black-box trajectory prediction model. *IEEE Transactions on Automation Science and Engineering*, 2024.
- Sun, Y., Guo, C., and Li, Y. React: Out-of-distribution detection with rectified activations. *Advances in Neural Information Processing Systems*, 34:144–157, 2021.
- Sun, Y., Ming, Y., Zhu, X., and Li, Y. Out-of-distribution detection with deep nearest neighbors. In *International Conference on Machine Learning*, pp. 20827–20840. PMLR, 2022.
- Szegedy, C. Intriguing properties of neural networks. *arXiv preprint arXiv:1312.6199*, 2013.
- Uesato, J., O’donoghue, B., Kohli, P., and Oord, A. Adversarial risk and the dangers of evaluating against weak attacks. In *International conference on machine learning*, pp. 5025–5034. PMLR, 2018.
- Van der Maaten, L. and Hinton, G. Visualizing data using t-sne. *Journal of machine learning research*, 9(11), 2008.

- Wang, H., Ge, S., Lipton, Z., and Xing, E. P. Learning robust global representations by penalizing local predictive power. *Advances in Neural Information Processing Systems*, 32, 2019.
- Wang, H., Xu, J., Xu, C., Ma, X., and Lu, J. Dissector: Input validation for deep learning applications by crossing-layer dissection. In *Proceedings of the ACM/IEEE 42nd International Conference on Software Engineering*, pp. 727–738, 2020.
- Xiao, K., Engstrom, L., Ilyas, A., and Madry, A. Noise or signal: The role of image backgrounds in object recognition. *arXiv preprint arXiv:2006.09994*, 2020.
- Xie, C., Huang, K., Chen, P.-Y., and Li, B. Dba: Distributed backdoor attacks against federated learning. In *International conference on learning representations*, 2019.
- Yang, J., Zhou, K., Li, Y., and Liu, Z. Generalized out-of-distribution detection: A survey. *International Journal of Computer Vision*, pp. 1–28, 2024.
- Yu, Y., Yang, Z., Wei, A., Ma, Y., and Steinhardt, J. Predicting out-of-distribution error with the projection norm. In *International Conference on Machine Learning*, pp. 25721–25746. PMLR, 2022.

A. Dataset split for each error source used in mentor training

As mentioned in [Sec. 3.3](#), for any given dataset of a mentor, let N_c and N_w represent the sets of n correctly and m incorrectly classified images by a mentee. The sizes of N_c and N_w can vary significantly, depending on the mentee’s classification performance. A mentee with high recognition accuracy will have more correct classifications (big n) and fewer incorrect ones (small m). To create a balanced test set for a mentor, we select equal numbers of correctly and incorrectly classified samples. The remaining samples are used for training. The details of the dataset split are shown in [Appendix, Tab. S1](#). To address the long-tail problem in the training set, during each training epoch for a mentor, we randomly generate a batch of samples that includes an equal number of correctly and incorrectly classified images by the mentee.

Table S1. Dataset split for each error source used in mentor training. If the mentor is trained on the mentee’s performance (ResNet50 or ViT) for a specific error source, the data in this error source will be split according to this table. N_{train} and N_{test} denote the number of training and testing samples, respectively, formatted as [number of samples misclassified by the mentee] / [number of samples correctly classified by the mentee].

Mentee	Error Source		CIFAR-10		CIFAR-100		ImageNet-1K	
			N_{train}	N_{test}	N_{train}	N_{test}	N_{train}	N_{test}
ResNet50	ID		151/9547	151/151	773/7681	773/773	5967/32099	5967/5967
	OOD	SpN	690/7930	690/690	1889/4333	1889/1889	9984/20048	9984/9984
		GaB	149/9553	149/149	760/7720	760/760	8013/25963	8012/8012
		Spat	222/9336	221/221	990/7032	989/989	7042/28874	7042/7042
		Sat	240/9282	239/239	1309/6072	1309/1309	8187/25439	8187/8187
	AA	Jitter	338/8988	337/337	1054/6840	1053/1053	7591/27227	7591/7591
		PGD	447/8661	446/446	1180/6460	1180/1180	9009/22973	9009/9009
		CW	487/8539	487/487	1120/6642	1119/1119	8102/25694	8102/8102
		PIFGSM	1613/5161	1613/1613	2090/3732	2089/2089	11226/16322	11226/11226
ViT	ID		128/9618	127/127	675/7977	674/674	4733/35801	4733/4733
	OOD	SpN	286/9144	285/285	1155/6535	1155/1155	6019/31945	6018/6018
		GaB	130/9610	130/130	678/7966	678/678	6402/30794	6402/6402
		Spat	170/9490	170/170	809/7573	809/809	5351/33947	5351/5351
		Sat	227/9319	227/227	1219/6345	1218/1218	5883/32351	5883/5883
	AA	Jitter	552/8344	552/552	1232/6304	1232/1232	10325/19025	10325/10325
		PGD	649/8053	649/649	1410/5770	1410/1410	14960/11680	11680/11680
		CW	446/8664	445/445	1136/6592	1136/1136	8614/24158	8614/8614
		PIFGSM	799/7605	798/798	1812/4564	1812/1812	15038/11654	11654/11654

B. Details of baselines

For performance comparison, we adopt seven baselines, as introduced in [Sec. 3.4](#). Their details are outlined below.

Self Error Rate (SER): We predict the correctness of the mentee’s outputs by referencing its accuracy on in-domain samples. For instance, if the mentee’s in-domain accuracy is 70%, we use a random binary generator that produces 1 (“correct”) with 70% probability and 0 (“wrong”) with 30% probability, applying this to all testing scenarios.

Maximum Class Probability (MCP) (Hendrycks & Gimpel, 2016): As mentioned in [Sec. 3.1](#), the mentee’s output logit is denoted as z_E . The maximum class probability of the mentee’s output is defined as $MCP(z_E) = \max \sigma(z_E)$ where $\sigma(\cdot)$ is the softmax function. The MCP indicates how confident the mentee is in its most probable prediction. We set a threshold γ to distinguish between the mentee’s confident and unconfident predictions. Specifically, if $MCP(z_E) > \gamma$, the mentee’s prediction will be considered a correct prediction due to its high confidence; otherwise, it will be regarded as an incorrect prediction. We employ three predefined thresholds for γ : 0.5, 0.7, and 0.9.

Class Probability Entropy (CPE): The class probability entropy of the mentee’s output is defined as $CPE(z_E) = H(\sigma(z_E))$, where $\sigma(\cdot)$ denotes the softmax function and $H(\cdot)$ represents the entropy measure quantifying the uncertainty in the probability distribution. A high entropy value signifies a high level of uncertainty in the mentee’s predictions. The entropy reaches its maximum value, $MaxCPE(z_E)$, when the mentee’s class probabilities in $\sigma(z_E)$ are equal. We define the uncertainty threshold as $\alpha \cdot MaxCPE(z_E)$, where $\alpha \in [0, 1]$. If $CPE(z_E) < \alpha \cdot MaxCPE(z_E)$, the mentee’s prediction is considered correct, indicating sufficient certainty in its prediction. Otherwise, the prediction is regarded as

incorrect. We set three predefined values for α : 0.01, 0.1 and 0.3.

Distance to centroid (DTC): The embedding generated by the mentee before the final binary classification layer represents the mentee’s feature interpretation of each sample. To determine the feature centroid for each class, we first average the features of all testing samples within that class based on the mentee’s predictions. Next, we calculate the L2 distance between each sample’s feature and its corresponding class centroid, denoted as d_s . We establish a distance threshold d ; if $d_s < d$, the mentee’s prediction is considered correct since the sample is close to the class centroid. Otherwise, the prediction is deemed incorrect. We have set three predefined values for d : 10, 20, and 30.

ConfidNet (Corbière et al., 2019): A shallow failure prediction neural network that learns True Class Probability (TCP) from the training set instead of relying on Maximum Class Probability (MCP).

TrustScore (Jiang et al., 2018): It introduces a new score called trust score by measuring the agreement between the classifier and a modified nearest-neighbor classifier on the testing samples for error prediction.

Steep Slope Loss (SSL) (Luo et al., 2021): Training an AI model for trustworthiness prediction by leveraging a carefully-designed steep slope loss function.

C. Example of calculating a mentor’s average accuracy using the proposed evaluation metric

As an example of computing the accuracy of a mentor evaluated using the metric presented in **Sec. 3.4**, we consider a mentor trained on C10-AA-PIFGSM and evaluate it on all the following datasets with their accuracies of 10% on C10-ID, 20% on C10-OOD-SpN, 30% on C10-OOD-GaB, 40% on C10-OOD-Spat, 50% on C10-OOD-Sat, 60% on C10-AA-Jitter, 70% on C10-AA-PGD, 80% on C10-AA-CW, and 90% on C10-AA-PIFGSM testing samples (See **Appendix, Tab. S1** for testing splits), the average accuracy of this mentor is calculated as $(10\% + 20\% + 30\% + 40\% + 50\% + 60\% + 70\% + 80\% + 90\%) / 9 = 50\%$. For simplicity, we refer to this average accuracy across all nine error sources as **Accuracy**. A mentor randomly guessing whether a mentee’s image classification is correct or incorrect for a given image would achieve an accuracy of 50%.

D. Joint training

As mentioned in **Sec. 4.1**, we add an experiment by training a Vision Transformer (ViT)-based mentor model on the correctness of a mixture of ID, OOD, and AA data for the ResNet-based mentee model from the CIFAR-10 dataset. The OOD data was corrupted with speckle noise, and the AA data was generated using PIFGSM. Compared to training the mentor solely on AA data which achieved an average accuracy of 78.0%, including ID and OOD data improved the average accuracy slightly to 79.1%. This minor improvement suggests a significant overlap of mentee error patterns among ID, OOD, and AA data. In other words, training mentors on OOD or ID data do not necessarily benefit mentors. Therefore, considering the associated computational costs, it is recommended to train mentors exclusively on AA data in practical applications. This finding underscores the significance of our study by providing critical insights into the optimal training practices for mentor models.

E. More comparisons between SuperMentor and baselines

As noted in the caption of **Tab. 1**, baseline performances across multiple hyperparameter configurations are indicated in **Appendix, Tab. S2**. In addition, when ViT serves as the mentee, the SuperMentor’s performance is shown in **Appendix, Tab. S3**. It can be seen that our SuperMentor can still achieve the best performance when the mentee has a backbone of ViT. This emphasizes the importance of the error source used during training.

Table S2. Performance comparison of baselines (multiple hyperparameter configurations) and our SuperMentor on various types of errors from the ImageNet-1K dataset. The ResNet50 model serves as the mentee, with its correctness of predictions evaluated by mentors. Best results are in bold.

	ID	SpN	GaB	Spat	Sat	PGD	CW	Jitter	PIFGSM	Average
SER	50.2	49.8	49.9	50.1	49.9	50.1	49.9	49.9	49.9	50.0
MCP ($\gamma = 0.5$)	69.5	73.5	73.6	72.2	71.7	66.0	66.7	65.1	64.9	69.2
MCP ($\gamma = 0.7$)	77.3	76.8	77.4	78.3	76.6	71.8	72.9	71.7	69.4	74.7
MCP ($\gamma = 0.9$)	78.2	73.3	74.5	77.0	74.9	72.2	72.3	73.0	69.0	73.8
CPE ($\alpha = 0.01$)	69.1	62.1	63.4	66.0	64.0	63.7	62.6	65.1	60.7	64.1
CPE ($\alpha = 0.1$)	78.0	75.2	75.9	78.0	76.2	72.2	72.8	72.7	69.3	74.5
CPE ($\alpha = 0.3$)	64.0	70.1	69.6	67.6	67.0	61.2	61.5	60.6	60.8	64.7
DTC ($d = 10$)	52.4	51.2	52.9	52.7	52.5	51.4	51.6	51.7	51.6	52.0
DTC ($d = 20$)	52.8	51.1	50.5	51.4	51.2	52.8	51.9	52.0	52.7	51.8
DTC ($d = 30$)	50.0	50.0	50.0	50.0	50.0	50.0	50.0	50.0	50.0	50.0
ConfidNet (Corbière et al., 2019)	67.3	65.9	68.5	70.8	67.9	68.8	69.0	70.1	67.1	68.4
TrustScore (Jiang et al., 2018)	70.0	67.5	71.1	73.4	71.3	73.2	72.5	73.9	72.7	71.7
SSL (Luo et al., 2021)	66.3	66.7	69.7	71.9	70.0	69.1	70.1	70.2	66.7	69.0
SuperMentor (ours)	78.9	73.6	74.6	78.3	73.6	83.0	78.4	79.9	72.3	77.0

Table S3. Performance comparison of baselines (multiple hyperparameter configurations) and our SuperMentor on various types of errors from the ImageNet-1K dataset. The ViT model serves as the mentee, with its correctness of predictions evaluated by mentors. Best results are in bold.

	ID	SpN	GaB	Spat	Sat	PGD	CW	Jitter	PIFGSM	Average
SER	49.9	50.0	49.9	49.9	50.0	49.8	50.0	49.9	50.0	49.9
MCP ($\gamma = 0.5$)	69.9	72.9	71.5	71.5	71.8	60.5	63.6	56.6	60.7	66.6
MCP ($\gamma = 0.7$)	78.5	77.9	78.0	78.1	78.0	63.9	67.8	61.5	63.8	71.9
MCP ($\gamma = 0.9$)	58.0	53.3	57.2	55.5	57.6	50.6	51.6	50.9	49.2	53.8
CPE ($\alpha = 0.01$)	50.0	50.0	50.0	50.0	50.0	50.0	50.0	50.0	50.0	50.0
CPE ($\alpha = 0.1$)	51.4	50.7	51.2	51.1	51.5	49.6	50.1	49.6	49.1	50.5
CPE ($\alpha = 0.3$)	72.4	73.7	73.5	72.7	73.5	61.3	63.7	57.0	60.2	67.5
DTC ($d = 10$)	69.5	68.9	69.3	68.6	68.6	65.7	64.1	61.8	67.0	67.1
DTC ($d = 20$)	50.9	50.4	50.4	50.6	50.6	50.2	50.3	50.2	50.3	50.4
DTC ($d = 30$)	50.0	50.0	50.0	50.0	50.0	50.0	50.0	50.0	50.0	50.0
ConfidNet (Corbière et al., 2019)	73.3	74.1	73.4	75.6	74.5	69.2	70.5	66.9	70.5	72.0
TrustScore (Jiang et al., 2018)	73.7	72.0	72.4	73.5	72.5	70.4	70.1	69.2	72.5	71.8
SSL (Luo et al., 2021)	64.3	66.3	68.2	70.6	69.3	62.5	66.0	60.1	62.4	65.5
SuperMentor (ours)	72.7	71.3	71.7	73.0	70.2	80.2	74.1	72.9	74.1	73.4

F. Ablation study

As mentioned in Sec. 4.5, we examine the effect of the distillation loss L_d (Fig. 2) on the SuperMentor performance. The results are presented in Appendix, Tab. S4. It is clear that excluding L_d results in a decrease in SuperMentor’s accuracy across all datasets. For example, in the C10 dataset, the average accuracy of SuperMentor decreases from 78.0% to 58.2%. This suggests that L_d encourages SuperMentor to learn the fine-grained decision boundaries among different object classes of a mentee.

Alternatively, instead of utilizing the mentee’s logits, SuperMentor can incorporate an additional cross-entropy loss to align the mentor’s predicted object class labels with those of the mentee, denoted as L_a . From Appendix, Tab. S4, we observe that replacing L_d with L_a leads to a slight decrease in accuracy. This is due to the fact that the mentee’s logits contain more information than the mentee’s class labels.

Table S4. **Ablation study of loss components in SuperMentor.** L_d denotes the distillation loss (see Sec. 3.1) and L_a represents the alignment loss between the mentor’s and mentee’s predicted class labels. SuperMentor is evaluated on a ResNet50 mentee. Results in each cell denote the average accuracy with the standard deviation over 3 runs. The performance of SuperMentor is highlighted in grey.

	L_d	L_a	ID	OOD				AA				Average
				SpN	GaB	Spat	Sat	PGD	CW	Jitter	PIFGSM	
C10	✗	✗	57.5±1.2	61.0±0.8	56.1±1.1	58.6±0.6	54.3±1.5	58.6±0.5	59.1±1.2	58.5±1.0	59.6±0.6	58.2±2.0
	✗	✓	80.0±1.8	73.7±0.6	79.2±2.0	77.9±0.8	74.3±1.9	80.5±0.8	76.5±0.8	79.7±0.7	71.2±0.4	77.0±3.2
		ours	80.9±1.6	73.2±0.7	80.5±1.4	79.4±1.3	75.6±1.0	81.4±0.9	78.2±0.9	80.7±1.2	71.9±0.1	78.0±3.5
C100	✗	✗	56.8±1.2	59.5±0.8	56.6±1.1	57.8±1.2	53.7±1.3	57.7±1.9	57.3±1.9	57.3±1.7	57.1±0.5	57.1±1.8
	✗	✓	75.0±0.7	70.9±0.3	74.8±0.7	74.1±0.3	68.1±0.8	78.1±0.6	75.2±0.6	76.2±0.5	66.5±1.0	73.2±3.7
		ours	75.4±0.7	71.1±0.1	75.4±0.6	74.5±0.8	68.4±1.1	78.3±0.4	75.6±0.4	76.6±0.2	66.9±0.4	73.6±3.7
IN	✗	✗	73.0±4.2	70.1±2.8	69.6±3.1	72.8±3.7	68.5±3.4	75.8±5.2	72.5±4.2	73.6±4.6	70.7±0.5	71.9±3.8
	✗	✓	78.7±0.1	73.1±0.2	73.6±0.5	78.0±0.1	73.2±0.3	83.0±0.1	78.4±0.1	79.9±0.1	72.2±0.2	76.7±3.6
		ours	78.9±0.0	73.6±0.1	74.6±0.2	78.3±0.1	73.6±0.2	83.0±0.1	78.4±0.1	79.9±0.0	72.3±0.1	77.0±3.4

G. Visualization

To gain an intuitive understanding of SuperMentor’s binary classification performance in error prediction, as mentioned in Sec. 4.5, we present the visualization of SuperMentor’s embeddings on three types of error sources of a mentee in Appendix, Fig. S1. It is evident that SuperMentor can effectively segregate samples correctly classified by the mentee from those that are misclassified, forming two distinct clusters.

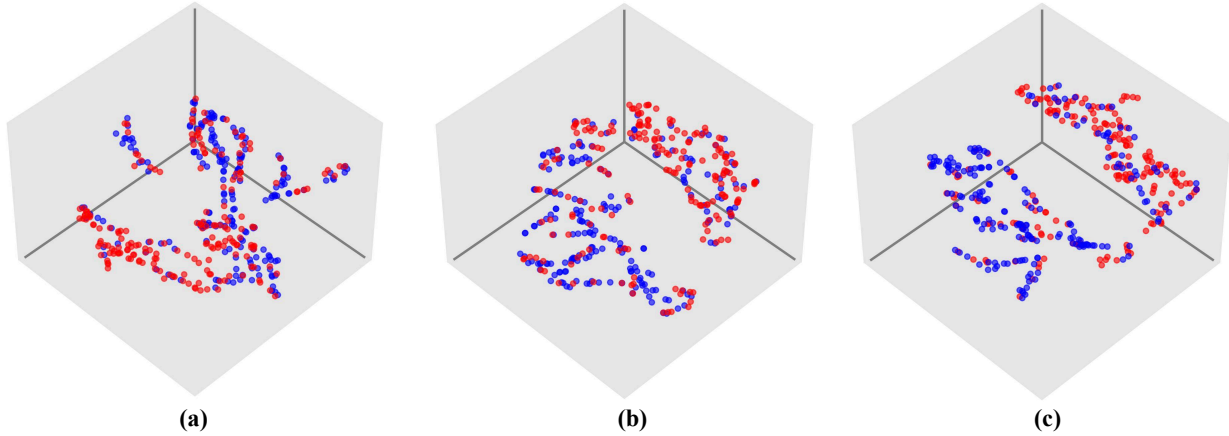


Figure S1. **3D visualization of the embeddings extracted from our SuperMentor Model for the classification of:** a) C10-ID samples, b) C10-OOD-GaB samples and c) C10-AA-Jitter samples. We use t-SNE (Van der Maaten & Hinton, 2008) to perform clusterings on the representations of our SuperMentor model for classifications of different error sources on the C-10 dataset. Red points indicate samples that the mentee fails to classify correctly, whereas blue points represent samples that the mentee successfully classifies. 200 red points and 200 blue points are randomly selected from the test sets and presented here. The visualized features are the embeddings computed based on the MLP in the second stream of the SuperMentor. Specifically, they are extracted before the final binary classification layer on whether the mentee makes a mistake.

H. SuperMentor in real-world practice

To reflect the real-world contribution of our work, as mentioned in Sec. 5, we expanded our experiments to the NCTCRCH100K (Kather et al., 2019) dataset which is used for medical image classification on colorectal cancer. This dataset comprises around 100K images across 9 tissue classes. Predicting AI models’ errors in medical image classification has significant real-world implications, such as reducing misdiagnoses and increasing the reliability of AI-assisted medical tools. Tab. S5 demonstrates that our SuperMentor accurately predicts the correctness of mentee outputs with an average

accuracy of 81.9%, significantly outperforming other baseline methods. This highlights that our proposed framework can offer greater value and reliability for AI error prediction compared to existing approaches in medical image classification.

Given the increasing integration of AI models into our daily lives, ensuring their accuracy is paramount, especially in high-stakes fields such as medicine and finance. This experiment with medical image datasets underscores the critical role that SuperMentor plays in enhancing reliability and trustworthiness in these vital areas, showcasing its potential to make a meaningful impact where precision and dependability are essential.

Table S5. Performance comparison of baselines (multiple hyperparameter configurations) and our SuperMentor on various types of errors from the NCTCRHE100K (Kather et al., 2019) dataset. The ResNet50 model serves as the mentee, with its correctness of predictions evaluated by mentors. Best results are in bold.

	ID	SpN	GaB	Spat	Sat	PGD	CW	Jitter	PIFGSM	Average
SER	49.8	49.6	50.4	50.0	49.9	50.1	50.2	49.8	49.8	50.0
MCP ($\gamma = 0.5$)	53.9	59.4	54.3	54.6	50.4	54.2	54.4	54.7	55.0	54.6
MCP ($\gamma = 0.7$)	65.1	71.3	65.0	66.2	49.9	66.2	66.1	65.8	67.1	64.7
MCP ($\gamma = 0.9$)	74.5	78.7	74.3	76.2	49.4	76.9	75.8	75.9	76.2	73.1
CPE ($\alpha = 0.01$)	78.5	74.2	81.9	77.7	45.2	77.4	77.4	77.8	77.3	74.2
CPE ($\alpha = 0.1$)	77.6	79.3	77.8	78.2	48.8	79.2	78.0	78.8	78.3	75.1
CPE ($\alpha = 0.3$)	67.6	76.3	67.0	68.8	51.7	70.3	69.0	69.9	69.5	67.8
DTC ($d = 10$)	77.7	67.3	77.2	79.7	66.2	78.8	77.4	77.6	78.1	75.5
DTC ($d = 20$)	69.4	48.5	67.2	61.6	52.4	59.2	64.7	62.2	59.2	60.5
DTC ($d = 30$)	52.6	49.4	53.2	50.7	50.0	51.1	52.4	51.5	50.9	51.3
ConfidNet (Corbière et al., 2019)	83.6	59.7	89.4	74.0	56.5	80.1	85.7	82.1	80.4	76.8
TrustScore (Jiang et al., 2018)	73.3	62.9	75.2	63.7	63.7	73.1	74.9	73.5	74.0	70.5
SSL (Luo et al., 2021)	79.3	57.1	87.4	75.9	56.9	76.2	83.1	77.7	76.9	74.5
SuperMentor (ours)	88.7	64.9	69.8	85.0	54.5	89.4	88.7	88.2	87.4	81.9

I. SuperMentor performance on additional OOD domains on ImageNet dataset

As mentioned in Sec. 5, we included experiments to evaluate the SuperMentor in more diversified OOD domains on ImageNet datasets, including ImageNet9-MIXED-RAND (IN9-MR) (Xiao et al., 2020), ImageNet9-MIXED-SAME (IN9-MS) (Xiao et al., 2020), ImageNet9-MIXED-NEXT (IN9-MN) (Xiao et al., 2020), ImageNet-R (IN-R) (Hendrycks et al., 2021) and ImageNet-Sketch (IN-S) (Wang et al., 2019). Specifically, the MIXED-RAND, MIXED-SAME, and MIXED-NEXT datasets are derived from 9 classes in ImageNet and contain varying amounts of background and foreground signals. These datasets aim to demonstrate that models often classify objects based on background cues (often spurious features), rather than the objects themselves. Specifically, MIXED-SAME, MIXED-RAND, and MIXED-NEXT represent images with random backgrounds from the same class, random backgrounds from a random class, and random backgrounds from the next class, respectively. The ImageNet-R dataset comprises images featuring artistic representations of objects, such as cartoons, community-generated art, and graffiti renditions. The ImageNet-Sketch dataset consists of sketch-like images that match the ImageNet validation set in both categories and scale.

To achieve a more thorough evaluation of our SuperMentor (see Sec. 4.5) in OOD domains, we assess its performance on these additional OOD datasets. It is worth noting that the SuperMentor learns from the mentee’s errors on adversarial ImageNet images generated by the PIFGSM attack only. In other words, the SuperMentor was NOT trained on any of these additional ImageNet-related OOD datasets. The SuperMentor achieves average accuracies of 68.46%, 69.24%, 67.04%, 58.68%, and 58.68% on the IN9-MR, IN9-MS, IN9-MN, IN-R, and IN-S datasets respectively, surpassing the 50% chance level. Despite that our Supermentor model is a simple ViT, it is still quite remarkable to achieve above-chance error prediction performance. We hope our work inspires researchers to explore more sophisticated AI mentors, incorporating advanced architectures or loss functions, to further enhance the ability to predict the correctness of another AI model’s outputs.

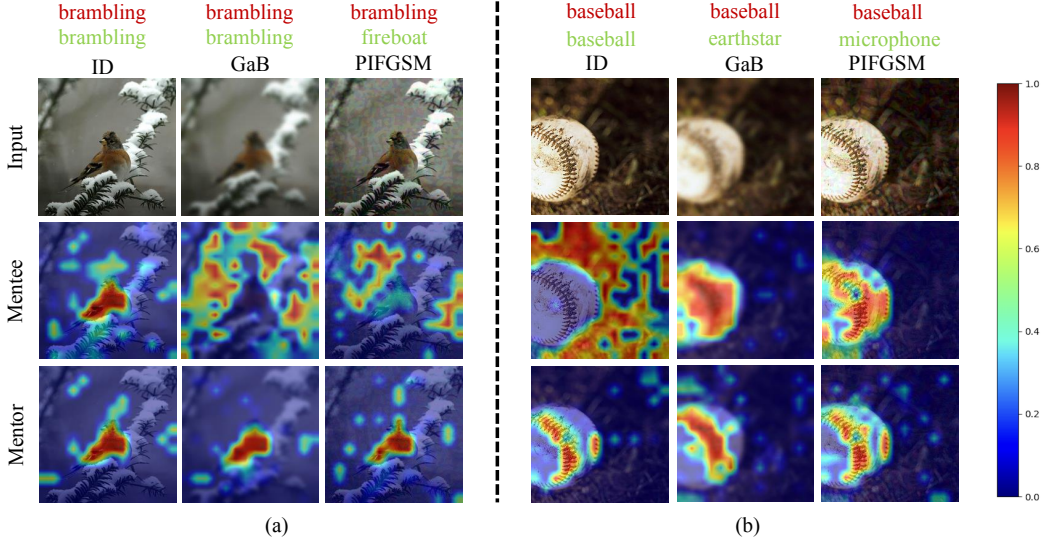


Figure S2. EigenCAM (Gildenblat & contributors, 2021; Muhammad & Yeasin, 2020) visualizations illustrating the behavior of our ViT SuperMentor and ViT mentee on sample images from the a) brambling and b) baseball classes in the IN-ID, IN-OOD-GaB, and IN-AA-PIFGSM datasets. The SuperMentor can accurately predict the correctness of the mentee’s predictions for these sample images. Each set of images is organized into three rows representing the input images (Input), EigenCAM visualization of the mentee’s prediction (Mentee), and EigenCAM visualization of the mentor’s prediction (Mentor), respectively. The first Layer Normalization module in the final transformer block of the Vision Transformer’s encoder is used as the mentor and mentee’s target visualization layer. The labels above each image column are Ground Truth Label and Mentee’s Prediction, respectively.

J. Discussion on the vulnerabilities of the mentor AI

Beyond error prediction, our framework improves the understanding of both individual and systemic vulnerabilities in Deep Neural Network (DNN)-based mentees, fostering more robust AI systems. This is further illustrated by the EigenCAM (Gildenblat & contributors, 2021; Muhammad & Yeasin, 2020) visualization in **Appendix, Fig. S2**. From these visualizations, we can make two observations below:

The vulnerabilities of the mentee do not overlap with those of the mentors. As illustrated in **Appendix, Fig. S2**, the mentor does not merely replicate the mentee’s learning patterns, as their activation maps for identical input images can differ significantly. For example, in the images shown in **Appendix, Fig. S2 (a)**, although the mentor and mentee exhibit very similar activation maps for ID images, their activations diverge greatly when the input image is corrupted by Gaussian Blur (GaB) or subjected to adversarial attacks using PIFGSM method. In the IN-OOD-GaB and IN-AA-PIFGSM images, the mentee demonstrates vulnerability under both corruption and adversarial attacks, whereas our SuperMentor does not exhibit such vulnerabilities on these OOD and AA images, consistently focusing on the brambling object. This indicates the vulnerabilities of mentors and mentees are distinct due to their non-overlapping objectives.

Our AI mentor serves as a valuable diagnostic tool for AI mentees. We argue that, beyond merely detecting errors, mentors function as important diagnostic tools for AI mentees, as supported in **Appendix, Fig. S2**. For example, in **Appendix, Fig. S2 (b)**, although the mentee correctly classifies the ID image, its activation map does not concentrate on the baseball but instead highlights background cues (spurious features). When the input image is corrupted by Gaussian Blur (GaB) or subjected to adversarial PIFGSM attacks, the mentee fails to make accurate predictions. In contrast, our SuperMentor effectively focuses on the stitches of the baseball—a key feature—regardless of whether the image is corrupted or adversarially attacked. The mentor highlights the stitches of the baseball as the key feature pattern that the mentee tends to overlook. This suggests that the mentor can identify vulnerabilities in the DNN-based model, even though it shares the same ViT architecture as the mentee. Furthermore, this reveals significant potential for our mentor to help refine the mentee’s performance by providing valuable insights into the mentee’s behavior.

In conclusion, **Appendix, Fig. S2** provides strong evidence that the AI mentor not only does not share the same vulnerabilities as the mentee but also serves as a valuable diagnostic tool for AI mentees.

K. Detailed performance of mentors across various error sources

As mentioned in the caption of **Fig. 3**, the detailed results of mentors across various error sources for the CIFAR-10, CIFAR-100, ImageNet-1K datasets are shown in **Appendix, Fig. S3, Fig. S4** and **Fig. S5** respectively.

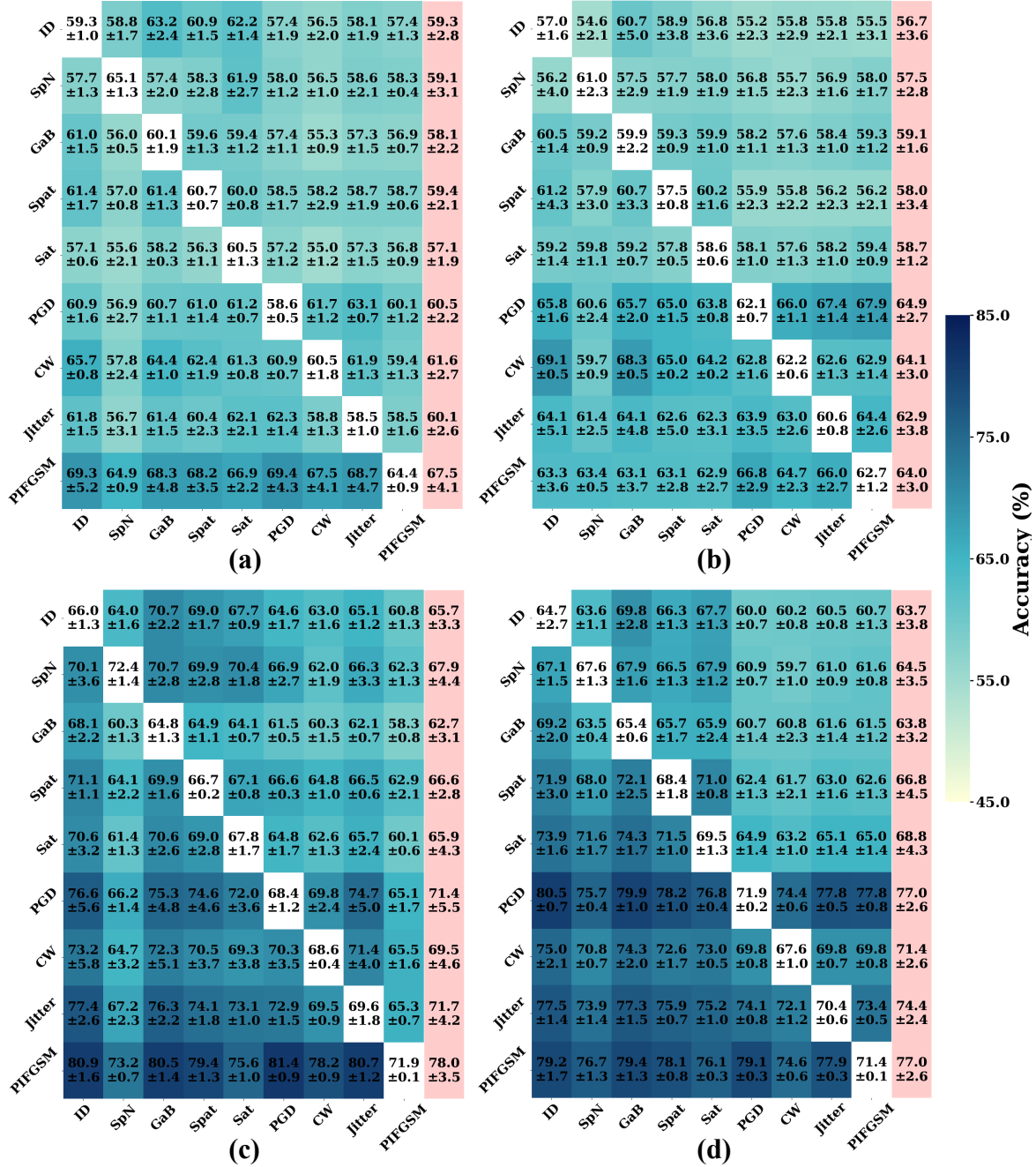


Figure S3. Heatmaps showing the average performance of mentor models across various error sources for the CIFAR-10 dataset, presented in the format [mentee]-[mentor]: a) ResNet50-ResNet50, b) ViT-ResNet50, c) ResNet50-ViT, and d) ViT-ViT. The heatmaps' row labels indicate the training error source for the mentor, while the column labels denote the testing error sources for the mentor. Results in each cell denote the average accuracy with the standard deviation over 3 runs. The pink-highlighted column displays the row-wise mean and standard deviation.

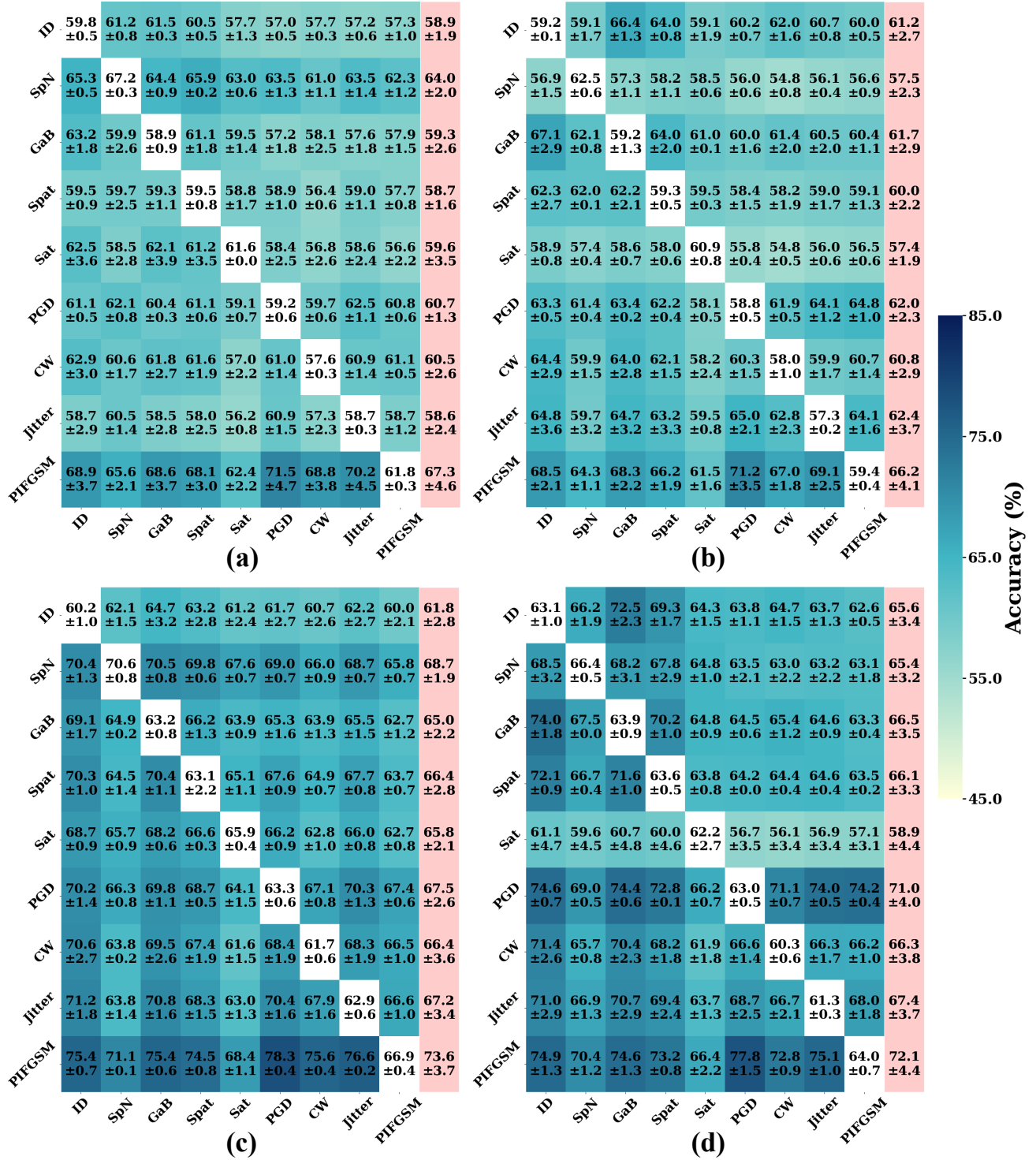


Figure S4. Heatmaps showing the average performance of mentor models across various error sources for the CIFAR-100 dataset, presented in the format [mentee]-[mentor]: a) ResNet50-ResNet50, b) ViT-ResNet50, c) ResNet50-ViT, and d) ViT-ViT. The heatmaps' row labels indicate the training error source for the mentor, while the column labels denote the testing error sources for the mentor. Results in each cell denote the average accuracy with the standard deviation over 3 runs. The pink-highlighted column displays the row-wise mean and standard deviation.

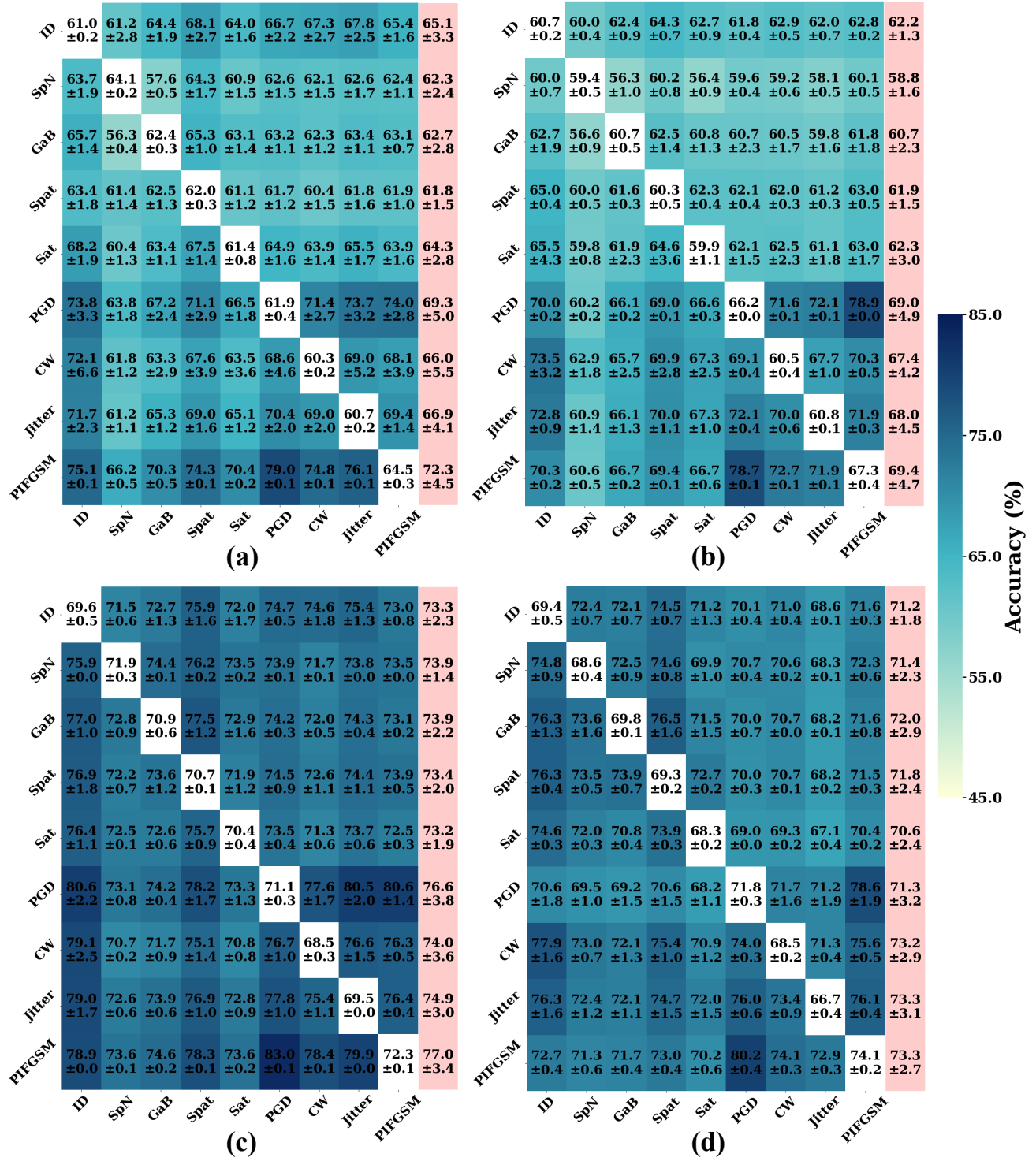


Figure S5. Heatmaps showing the average performance of mentor models across various error sources for the ImageNet-1K dataset, presented in the format [mentee]-[mentor]: a) ResNet50-ResNet50, b) ViT-ResNet50, c) ResNet50-ViT, and d) ViT-ViT. The heatmaps' row labels indicate the training error source for the mentor, while the column labels denote the testing error sources for the mentor. Results in each cell denote the average accuracy with the standard deviation over 3 runs. The pink-highlighted column displays the row-wise mean and standard deviation.

L. Detailed performance of mentors across mentee architectures

In **Fig. 5**, we show the generalization performance of mentors averaged over all three error types of mentees with various architectures. Here, we expand the results in the form of tables listing out all the individual accuracy for all the error sources on CIFAR-10, CIFAR-100 and ImageNet-1K datasets in **Appendix, Tab. S6, Tab. S7, and Tab. S8** respectively.

Table S6. Detailed generalization performance of mentors across various mentee architectures on error sources from the CIFAR-10 dataset. The mentee rows are formatted as [mentee A]→[mentee B], as explained in **Fig. 5**. Results in each cell denote the average accuracy with the standard deviation over 3 runs.

Mentor		ResNet50		ViT	
Mentee		ResNet50→ViT	ViT→ResNet50	ResNet50→ViT	ViT→ResNet50
ID		59.3±2.8→59.6±2.0	56.7±3.6→54.5±2.4	65.7±3.3→65.6±3.4	63.7±3.8→62.5±3.0
OOD	SpN	59.1±3.1→58.4±3.3	57.5±2.8→57.4±2.1	67.9±4.4→66.1±5.0	64.5±3.5→62.9±2.7
	GaB	58.1±2.2→58.2±2.0	59.1±1.6→57.3±1.8	62.7±3.1→62.4±2.8	63.8±3.2→62.6±2.8
	Spat	59.4±2.1→58.4±2.1	58.0±3.4→57.4±3.0	66.6±2.8→66.1±3.7	66.8±4.5→65.2±3.8
	Sat	57.1±1.9→57.7±1.3	58.7±1.2→56.7±1.8	65.9±4.3→66.4±3.2	68.8±4.3→67.7±4.3
AA	PGD	60.5±2.2→58.4±1.5	64.9±2.7→62.3±1.7	71.4±5.5→69.0±4.5	77.0±2.6→72.3±4.1
	CW	61.6±2.7→59.2±2.2	64.1±3.0→60.3±2.0	69.5±4.6→67.7±4.0	71.4±2.6→67.6±3.1
	Jitter	60.1±2.6→59.3±1.8	62.9±3.8→60.1±3.3	71.7±4.2→70.4±3.5	74.4±2.4→70.4±3.8
	PIFGSM	67.5±4.1→65.3±3.4	64.0±3.0→62.1±2.3	78.0±3.5→75.4±3.4	77.0±2.6→72.5±3.9
Average		60.3±3.9→59.4±3.2	60.7±4.2→58.7±3.4	68.8±5.9→67.7±5.1	69.7±6.2→67.1±5.2

Table S7. Detailed generalization performance of mentors across various mentee architectures on error sources from the CIFAR-100 dataset. The mentee rows are formatted as [menteeA]→[menteeB], as explained in **Fig. 5**. Results in each cell denote the average accuracy with the standard deviation over 3 runs.

Mentor		ResNet50		ViT	
Mentee		ResNet50→ViT	ViT→ResNet50	ResNet50→ViT	ViT→ResNet50
ID		58.9±1.9→58.4±1.8	61.2±2.7→60.1±2.1	61.8±2.8→61.4±2.9	65.6±3.4→63.8±2.0
OOD	SpN	64.0±2.0→61.8±3.5	57.5±2.3→57.9±2.9	68.7±1.9→65.1±3.2	65.4±3.2→64.6±2.6
	GaB	59.3±2.6→58.6±2.0	61.7±2.9→61.0±1.9	65.0±2.2→63.8±2.5	66.5±3.5→64.6±1.9
	Spat	58.7±1.6→57.7±1.9	60.0±2.2→59.5±2.0	66.4±2.8→64.9±2.7	66.1±3.3→64.0±2.0
	Sat	59.6±3.5→58.8±3.4	57.4±1.9→57.4±2.6	65.8±2.1→64.4±3.0	58.9±4.4→58.4±4.4
AA	PGD	60.7±1.3→59.4±1.1	62.0±2.3→60.6±1.3	67.5±2.6→65.5±2.0	71.0±4.0→67.2±2.1
	CW	60.5±2.6→59.2±1.8	60.8±2.9→58.9±2.1	66.4±3.6→64.5±2.1	66.3±3.8→63.6±1.8
	Jitter	58.6±2.4→57.8±2.0	62.4±3.7→60.5±2.4	67.2±3.4→65.2±2.2	67.4±3.7→65.1±1.9
	PIFGSM	67.3±4.6→64.6±2.5	66.2±4.1→64.3±2.2	73.6±3.7→69.1±1.7	72.1±4.4→68.5±2.3
Average		60.8±3.9→59.6±3.2	61.0±3.8→60.0±2.9	66.9±4.1→64.9±3.2	66.6±5.2→64.4±3.6

Table S8. Detailed generalization performance of mentors across various mentee architectures on error sources from the ImageNet-1K dataset. The mentee rows are formatted as [menteeA]→ [menteeB], as explained in Fig. 5. Results in each cell denote the average accuracy with the standard deviation over 3 runs.

Mentor		ResNet50		ViT	
Mentee		ResNet50→ ViT	V→ ResNet50	ResNet50→ ViT	ViT→ ResNet50
ID		65.1±3.3→ 63.9±2.7	62.2±1.3→ 62.5±1.6	73.3±2.3→ 71.0±2.4	71.2±1.8→ 71.5±1.4
OOD	SpN	62.3±2.4→ 62.0±3.7	58.8±1.6→ 58.4±2.2	73.9±1.4→ 71.1±2.2	71.4±2.3→ 71.2±1.3
	GaB	62.7±2.8→ 62.9±3.8	60.7±2.3→ 60.5±2.7	73.9±2.2→ 71.8±3.0	72.0±2.9→ 71.5±1.7
	Spat	61.8±1.5→ 61.1±1.7	61.9±1.5→ 61.7±1.4	73.4±2.0→ 71.4±2.3	71.8±2.4→ 71.7±1.4
	Sat	64.3±2.8→ 63.9±3.5	62.3±3.0→ 62.1±2.7	73.2±1.9→ 71.2±2.6	70.6±2.4→ 70.3±1.2
AA	PGD	69.3±5.0→ 66.8±2.6	69.0±4.9→ 67.1±2.7	76.6±3.8→ 72.6±2.0	71.3±3.2→ 70.3±1.6
	CW	66.0±5.5→ 64.3±3.5	67.4±4.2→ 65.8±2.3	74.0±3.6→ 71.1±1.9	73.2±2.9→ 71.7±1.4
	Jitter	66.9±4.1→ 65.3±2.5	68.0±4.5→ 66.1±2.6	74.9±3.0→ 72.2±2.0	73.3±3.1→ 71.3±1.3
	PIFGSM	72.3±4.5→ 69.3±2.2	69.4±4.7→ 68.0±2.9	77.0±3.4→ 72.9±1.7	73.3±2.7→ 72.1±1.4
Average		65.6±5.0→ 64.4±3.8	64.4±5.1→ 63.6±3.9	74.4±3.0→ 71.7±2.4	72.0±2.8→ 71.3±1.5